Analysis of the origin of the distribution of CO in the subtropical southern Indian Ocean in 2007

V. Duflot,[1] B. Dils,[2] J. L. Baray,[1] M. De Mazière,[2] J. L. Attié,[3,4] G. Vanhaelewyn,[2] C. Senten,[2] C. Vigouroux,[2] G. Clain,[1] and R. Delmas[1]

Received 2 February 2010; revised 19 July 2010; accepted 28 July 2010; published 17 November 2010.

[1] We show carbon monoxide (CO) distributions at different vertical levels over the subtropical southern Indian Ocean, analyzing an observation campaign using Fourier transform infrared (FTIR) solar absorption spectrometry performed in 2007 at Reunion Island (21°S, 55°E). The CO pollution levels detected by the FTIR measurements during the campaign show a doubling of the CO total columns during the Southern Hemisphere biomass burning season. Using correlative data from the Measurement of Pollution in the Troposphere instrument and back trajectories analyses, we show that the potential primary sources for CO throughout the troposphere in 2007 are southern Africa (June–August) and South America (September–October). A secondary potential contribution from Southeast Asia and Indonesia-Malaysia was identified in the upper troposphere, especially in July and September. We examine the relation between the Asian monsoon anticyclone seasonal cycle and this result. We also investigate the relative contribution of different areas across the globe to the CO concentration in the subtropical southern Indian Ocean in 2007 using backward simulations combining the Lagrangian model FLEXPART 6.2, the Global Fire Emissions Database (GFEDv2.1) and the Emission Database for Global Atmospheric Research (EDGARv3.2-FT2000). We confirm the predominance of the African and South American contributions in the CO concentration in the southern subtropical Indian Ocean below 11 km. We show that CO transported from Australia makes only a small contribution to the total CO concentration observed over Reunion Island, and that the long-range transport of CO coming from Southeast Asia and Indonesia-Malaysia is important, especially from June until September in the upper troposphere.

Citation: Duflot, V., B. Dils, J. L. Baray, M. De Mazière, J. L. Attié, G. Vanhaelewyn, C. Senten, C. Vigouroux, G. Clain, and R. Delmas (2010), Analysis of the origin of the distribution of CO in the subtropical southern Indian Ocean in 2007, *J. Geophys. Res.*, *115*, D22106, doi:10.1029/2010JD013994.

1. Introduction

[2] Carbon monoxide (CO) is an atmospheric pollutant produced by oxidation of methane and other biogenic hydrocarbons, fossil fuel combustion, biofuel use, and biomass burning (BB) [*Galanter et al.*, 2000; *Intergovernmental Panel on Climate Change*, 2001], the latter two being the major sources in tropical areas. CO is a precursor of ozone (O_3) [*Daniel and Solomon*, 1998], especially in the tropical lower troposphere because of an abundance of water vapor (H_2O) and the strong solar flux [*Ridley et al.*, 1992], and can affect the oxidizing capacity of the atmosphere by reacting with the hydroxyl (OH) radical [*Logan et al.*, 1981; *Kanakidou and Crutzen*, 1999]. Aside from its chemical properties, CO is an interesting tracer for studying atmospheric transport: having a lifetime of weeks to a few months, it is an effective indicator of how the large-scale distribution of atmospheric pollutants is influenced by long-range transport of biomass and fossil fuel burning.

[3] At Reunion Island in the subtropical southern Indian Ocean (21°S, 55°E), the influence of BB on the tropical tropospheric composition and the associated transport schemes has been mainly determined by analyzing O_3 measurements [*Randriambelo et al.*, 2000; *Clain et al.*, 2009]. However, it is difficult in case of O_3 to distinguish between the contributions of anthropogenic sources and the contributions of stratosphere-troposphere exchange which can be induced, in this region, by the subtropical jet stream [*Baray et al.*, 1998] and by the tropical convection [*Zachariasse et al.*, 2000; *Leclair De Bellevue et al.*, 2006]. Since CO is mainly produced in the lower troposphere, investigating its distribution in the

[1]Laboratoire de l'Atmosphère et des Cyclones, Université de la Réunion, UMR CNRS-Météo-France 8105, Saint-Denis de la Réunion, France.
[2]Institut d'Aéronomie Spatiale de Belgique, Brussels, Belgium.
[3]Laboratoire d'Aérologie, UMR 5560, Université de Toulouse, CNRS/UPS, Toulouse, France.
[4]CNRM-GAME Météo-France and CNRS URA 1357, Toulouse, France.

0148-0227/10/2010JD013994

subtropical southern Indian Ocean increases our understanding of pollutant transport phenomena. *Bremer et al.* [2004] pointed out that on Reunion Island, O_3 columns are highest in September–October, in phase with the CO peak occurring in this period because of BB in South Africa and Madagascar. High concentrations of O_3 precursors from these fires are vented into the upper troposphere by deep convection and are subsequently advected into the Indian Ocean region by westerly winds. The 2000 Southern African Regional Science Initiative (SAFARI 2000 [*Annegarn et al.*, 2002; *McMillan et al.*, 2003; *Swap et al.*, 2003]) indicated that low-latitude transport of biomass burning pollution from the African continent to the Indian Ocean takes place along in the "river of smoke" exiting southern Africa. The biomass burning pollution from Africa could be traced as far as southeast Australia [*Pak et al.*, 2003] and likely contributed to the enhanced CO levels observed by the Measurement of Pollution in the Troposphere (MOPITT) instrument at Reunion Island [*Bremer et al.*, 2004]. Moreover, *Edwards et al.* [2006a] have shown that the Southern Hemisphere (SH) transport is governed to a large extent by the three anticyclonic circulations over the Atlantic Ocean, the African continent, and the Indian Ocean that are dominant features during austral spring. They also pointed out that southern African BB emissions mostly find their way into the Indian Ocean and follow the five transportation modes identified by *Garstang et al.* [1996]. In addition, a recent study based on CO observations by the Aura Microwave Limb Sounder (MLS), airborne Measurement of Ozone and Water Vapor by Airbus In-Service Aircraft (MOZAIC) observations, and the chemistry transport model Modélisation de la Chimie Atmosphérique Grande Echelle (MOCAGE) has shown episodes of transport of CO in the Northern Hemisphere (NH) coming from eastern Asia and reaching northern Africa's upper troposphere during the Asian summer monsoon (ASM) [*Barret et al.*, 2008]. Using a chemistry general circulation model and Indian Ocean Experiment (INDOEX) data obtained during February and March 1999, *De Laat et al.* [2001] report that CO from India and Southeast Asia is advected in the marine boundary layer toward the Intertropical Convergence Zone (ITCZ), where it is lifted into the free troposphere by convection. At high tropospheric altitudes, CO spreads out, with most of it being transported back to the NH, and only a small part ends up getting mixed into the SH.

[4] These studies have documented the CO distribution and sources in the Indian Ocean, but the limited vertical resolution of the satellite retrievals and the few in situ measurement stations in this area are inadequate to yield a more detailed CO vertical distribution. Furthermore, some evidence of the possibility of transport of Southeast Asian CO far from the emission sources into the subtropical southern Indian Ocean has been put forward during late austral summer [*De Laat et al.*, 2001], but their occurrence during austral winter and their impact on the contaminated area still have to be investigated.

[5] Being located in the subtropical southern Indian Ocean at around 800 km east of Madagascar, Reunion Island is a good location to study the effect of long-range transport on the southern Indian Ocean atmospheric composition. Two measurement campaigns with Fourier transform infrared (FTIR) solar absorption spectrometry have been performed at Reunion Island in 2002 and 2004 covering the end of the SH BB season (October 2002 and August to October 2004). A third FTIR campaign was organized from May to October 2007 to obtain measurements before and during the whole SH BB season. Using the acquired data, *Senten et al.* [2008] and *Vigouroux et al.* [2009] were able to detect the seasonal variation of CO and HCHO in the SH BB season, as well as the impact of particular BB events in Africa and Madagascar on the atmospheric composition above Reunion Island.

[6] The objectives of this paper are to document the time evolution of the vertical distribution of the abundance of CO above Reunion Island in 2007, to determine the sources which govern this time evolution, and to examine if air masses coming from Southeast Asia can be identified and how they affect the CO distribution in the subtropical southern Indian Ocean area. In this work, we exploit the FTIR measurements of CO from the 2007 campaign in combination with global fire pixels from the Moderate Resolution Imaging Spectroradiometer (MODIS) and MOPITT remote sensing data for detecting fires and monitoring CO concentrations, respectively. We have also performed a set of back trajectory simulations to investigate the origin of the air masses passing over Reunion Island and a set of backward simulations combining the Lagrangian model FLEXPART, the Global Fire Emissions Database (GFEDv2.1), and the Emission Database for Global Atmospheric Research (EDGARv3.2-FT2000) to evaluate the relative contribution from different emission areas.

[7] Section 2 describes the FTIR experiments and the CO retrieval method, the MOPITT and MODIS data as well as the back trajectory calculation software, the FLEXPART model and the GFED and EDGAR databases. In section 3, we show the results of the FTIR CO retrievals and MOPITT measurements in order to describe the evolution of the CO abundance and vertical distribution in the subtropical southern Indian Ocean area. The dynamical processes that govern this CO distribution are discussed in section 4, and the relative contributions of different areas across the globe to CO variations observed at Reunion Island in 2007 are detailed in section 5.

2. Experiments and Models

2.1. FTIR Campaigns and Retrievals of CO Vertical Profiles

[8] The solar absorption FTIR experiments were performed using a Bruker 120M interferometer. The instrument was installed in a temperature-controlled container placed on the roof of a building at the University of Reunion Island campus at Saint-Denis (50 m above sea level, 20°54′S and 55°29′E). Solar absorption measurements were performed from 8 August until 25 October 2004 and from 24 May until 15 October 2007, whenever the sky was clear. The spectra were recorded between 600 and 4300 cm^{-1} (2300 to 17000 nm) with a maximal spectral resolution of 0.0036 cm^{-1} (0.0143 nm) (maximum optical difference = 250 cm).

[9] The FTIR experiment configuration and technical features for the 2004 campaign are described in *Senten et al.* [2008]; the FTIR 2007 campaign configuration was almost identical.

[10] CO total column amounts and volume mixing ratio (vmr) profiles were retrieved using the Spectral Least Squares Fitting (SFIT-2) algorithm using the optimal estimation method developed by *Rodgers* [2000]. A detailed description

Table 1. Summary of the Retrieval Characteristics for CO for the FTIR Campaigns at Reunion Island[a]

Molecule	CO
Microwindows (cm^{-1})	2057.70–2057.91 2069.55–2069.72 2157.40–2159.20 2140.40–2141.40 2165.37–2165.85 2168.84–2169.02
Variability (%)	20%
SNR	150
HWHM (km)	4
Spectral resolution (cm^{-1})	0.0036
Interfering species	O_3, OCS, CO_2, N_2O, H_2O, solar CO
DOFS mean	2.96 (2004); 3.06 (2007)

[a]Variability represents the diagonal elements of the a priori profile's covariance matrix (Sa) and HWHM the interlayer correlation length in Sa. The first, fifth, and sixth rows list the spectral microwindows that are fitted simultaneously, the associated spectral resolution, and the main interfering species. SNR is the ad hoc signal-to-noise ratio adopted in the retrievals. The last row provides the mean DOFS achieved in 2004 and 2007.

of the SFIT-2 program can be found in *Senten et al.* [2008] and references therein.

[11] In the current work, the retrieval strategy for CO was slightly improved compared to the one described in *Senten et al.* [2008] in order to increase the degrees of freedom for signal (DOFS) [*Rodgers*, 2000] and improve the retrieval error budget. Table 1 lists the most important retrieval parameters: the microwindows in which the spectra were analyzed and the interfering molecules which were fitted simultaneously by profile scaling as well as the spectral resolution and effective signal-to-noise ratio (SNR). Also listed are the diagonal elements and the half-widths at half-maximum defining the Gaussian interlayer correlation length of the a priori profile's covariance matrix adopted in the retrieval. The a priori profile is the same as in *Senten et al.* [2008]. The achieved mean DOFS are 2.96 and 3.06 for the 2004 and 2007 campaigns, respectively, indicating that there are approximately three independent pieces of information contained in the measurement. In order to exploit the FTIR profiles, it is necessary to determine to which extent the retrievals in each altitude layer result from the measurement, meaning not from the a priori profile, and are uncorrelated to the other layers. The eigenvectors and associated eigenvalues of the averaging kernel matrix provide this information: the structures in the profile corresponding to these eigenvectors can be thought of as being measured independently [*Rodgers*, 2000]. In Figure 1a we show the three most representative eigenvectors of the averaging kernels matrix for the 2004 and 2007 campaigns, associated to the three largest eigenvalues. The vectors' shapes depict the CO profile's independent layers that can be considered: 0–5 km, 5–11 km, and 11–17 km. Figure 1b presents the averaging kernels corresponding to each of these three layers. The FTIR measurements are especially sensitive to the 0–3 km, 7–11 km, and 13–17 km layers. Figure 1c shows the so-called sensitivity curve, which, at each altitude, corresponds to the sum of the averaging kernel elements for that altitude. We can see in Figure 1 that measurements contribute more than 90% to the retrievals up to about 17 km. Hence, in the remainder of this paper information from FTIR will only be taken into account up to 17 km.

[12] Table 2 summarizes the evaluation of the error budget for the 2007 FTIR campaign data. Evaluation of the error budget for the 2004 FTIR campaign data as well as the description of each contribution and details about their calculation can be found in *Senten et al.* [2008].

2.2. Data and Back Trajectory Models

2.2.1. MODIS Fire Detection

[13] The MODIS instrument on board the Terra and Aqua satellites (http://modis.gsfc.nasa.gov/) enables active fire detection based on the high infrared emissions of the fires [*Giglio et al.*, 2003]. This information is available via the Fire Information for Resource Management System (FIRMS) site developed by the University of Maryland (http://maps.geog.umd.edu/firms/). FIRMS delivers active fire spots using the MODIS active fire locations processed by the MODIS Rapid Response System using the standard MODIS MOD14 Fire and Thermal Anomalies product. Each active fire location represents the center of a 1 km pixel that is flagged by the algorithm as containing a fire within the pixel.

2.2.2. MOPITT

[14] MOPITT (http://www.acd.ucar.edu/mopitt/) [*Drummond and Mand*, 1996] is a nadir-pointing instrument on NASA's EOS Terra spacecraft that has been operational since March 2000, measuring tropospheric CO on the global scale. The ground pixel size (or footprint) is 22 × 22 km, and the vertical profiles are retrieved on seven pressure levels (surface, 850, 700, 500, 350, 250, and 150 hPa). MOPITT CO retrievals are based on the maximum likelihood method, which uses a statistical combination of the measurements and a priori information [*Rodgers*, 2000]. In this study, we consider MOPITT CO (version 3) daytime retrievals which have a better DOFS than nighttime retrievals [*Deeter et al.*, 2004a]. Furthermore, only retrievals with less than 50% a priori contamination are exploited to ensure a consistent and good quality of the data set.

[15] MOPITT retrievals provide average CO values in two relatively broad layers of the atmosphere: in the lower troposphere from about 850 to 500 hPa, and in the upper troposphere from about 300 to 200 hPa [*Deeter et al.*, 2004a; *Kar et al.*, 2004]. Detailed reports on validation exercises can be found in *Deeter et al.* [2004b] and *Emmons et al.* [2004, 2007, 2009]. Figure 2 shows the 700 and 250 hPa MOPITT-averaging kernels in 2007 over a surface of 300 km diameter around Reunion Island. The averaging kernels have been grid normalized with respect to the considerations stated in *Deeter et al.* [2007]. Because of the size of Reunion Island being ~72 km across, the MOPITT retrievals over Reunion Island are mainly retrievals over sea which reduces the MOPITT sensitivity to the low troposphere [*Deeter et al.*, 2007]. One can see on Figure 2 that the 700 hPa MOPITT retrievals are mainly impacted by the CO concentration in the ~2–8 km (~850–350 hPa) layer while the 250 hPa retrievals are representative of the CO concentration in the ~8–13 km (~350–150 hPa) layer.

2.2.3. FLEXPART, GFED, and EDGAR

[16] FLEXPART version 6.2 is a Lagrangian particle dispersion model [*Stohl et al.*, 1998, 2005], which simulates the transport and dispersion of linear tracers and treats advection and turbulent diffusion by calculating the trajectories for a multitude of particles. Stochastic fluctuations, obtained by solving Langevin equations [*Stohl and Thompson*, 1999], are

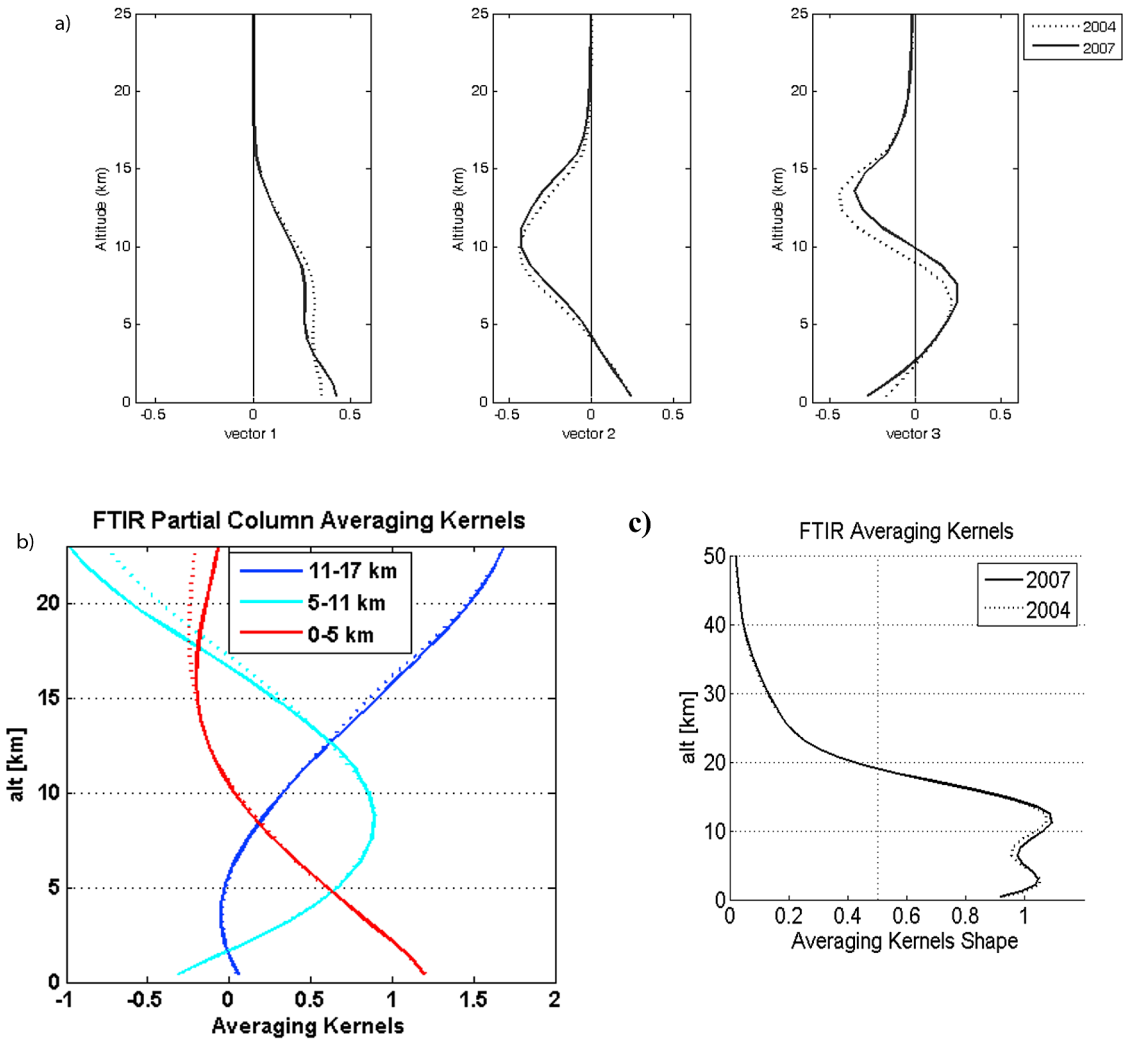

Figure 1. (a) FTIR eigenvectors of the 2004 (dotted lines) and 2007 (solid lines) averaging kernels matrices respectively associated to the eigenvalues 0.99, 0.98, and 0.78 (2004) and 0.99, 0.97, and 0.71 (2007). For both campaigns, the first eigenvector gives the 0–5 km independent layer while vectors 2 and 3 give the 5–11 km and 11–17 km independent layers. (b) FTIR CO partial columns' averaging kernels (in mol cm^{-2}/mol cm^{-2} dimensionless units) for the 2004 (dotted lines) and 2007 (solid lines) campaigns. (c) FTIR sensitivity curve for the 2004 (dotted lines) and 2007 (solid lines) campaigns.

superimposed on the grid-scale winds from the European Centre for Medium-Range Weather Forecasts (ECMWF) data set to represent transport by turbulent eddies. The FLEXPART model was driven by global wind field data from ECMWF, with a spatial resolution of 1° × 1° and a temporal resolution of 3 h. The back trajectories calculation period has been set to 50 days. This period might be too long for lower tropical CO lifetimes, but it is adequate for the higher troposphere where lifetimes are longer.

Table 2. Summary of the Error Budget Evaluations (%) for the Total and Partial Columns From the 2007 FTIR Campaign Data[a]

Columns (km)	Temperature Error	Interfering Species Error	FM Parameters Error	Measurement Error	Smoothing Error	Solar Angle Error	Total Random Error	Line Intensity Error	Air Broadening Error	Total Systematic Error
0–5	2.26	0.31	1.03	0.73	3.81	0.36	4.63	4.29	3.55	5.57
5–11	0.86	0.43	1.62	1.25	5.18	0.32	5.66	5.94	4.23	7.29
11–17	0.45	0.50	1.54	1.79	4.97	0.37	5.55	11.78	3.79	12.37
17–100	1.35	1.74	0.44	1.71	6.51	0.16	7.09	8.26	1.50	8.40
0–100	1.10	0.06	0.27	0.15	0.11	0.34	1.20	2.40	0.42	2.44

[a]The listed error contributions are (from left to right): temperature error, interfering species error, forward model parameters error, measurement noise error, smoothing error, solar zenith angle error, total random error, line intensity error, air broadening error, and total systematic error.

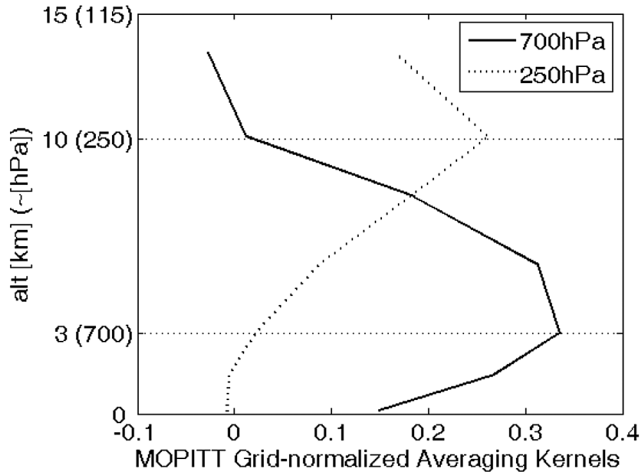

Figure 2. Grid-normalized MOPITT averaging kernels (in vmr/vmr dimensionless units) over Reunion Island for the 700 hPa (solid line) and 250 hPa (dotted line) retrieval levels.

[17] GFEDv2.1 [*van der Werf et al.*, 2006] consists of 8-day time step 1° × 1° degree gridded fire emissions of CO. The data set was compiled using satellite data and the Carnegie-Ames-Stanford approach (CASA) biogeochemical model.

[18] EDGAR stores global emission inventories of greenhouse gases and air pollutants from anthropogenic sources. We used in this paper anthropogenic CO emissions from EDGARv3.2-FT2000 (year 2000) [*Olivier et al.*, 2005]. The EDGARv3.2-FT2000 data is available on a 1° × 1° grid.

2.2.4. LACYTRAJ

[19] LACYTRAJ is a kinematic back trajectory code using ECMWF wind fields. This code is used to determine the sources of the air masses arriving above Reunion Island. The back trajectories presented in this paper were calculated using a 15 min time step. The start grid is defined with 0.5° latitude and longitude steps around Reunion Island, and the maximum period that has been used for calculation of the back trajectories is 10 days. This duration is long enough to reach areas as far as South America. Details on this code can be found in *Clain et al.* [2010].

3. Observed Total Columns and Vertical Distributions of CO in the Subtropical Southern Indian Ocean

3.1. Ground-Based FTIR Observations at Reunion Island

[20] The time series of CO total columns retrieved from FTIR solar absorption measurements at Reunion Island during the 2007 campaign are shown in Figure 3; 2004 campaign data are included in Figure 3 for comparison. During the 2007 campaign, a stable CO background concentration around $1.5 \pm 0.07 \times 10^{18}$ molecules/cm^2 is observed until the beginning of August. Later, a significant increase in the total columns occurs during both campaigns, with peaks in October corresponding to twice the CO background concentration ($\sim 3 \pm 0.15 \times 10^{18}$ molecules/cm^2) measured during June to mid-August. The major sink for CO is reaction with OH radicals. High UV and humidity promote the formation of OH radicals from the photolysis of O_3 [*Logan et al.*, 1981; *Thompson*, 1992] during tropical summer. The CO lifetime is then longer in winter, and CO could accumulate. However, this cannot explain the observed CO increase: the period studied here (June to October 2007) is an austral winter time period, so the CO lifetime has already been lengthened. The observed CO increase coincides with the known SH BB seasonality: BB emissions occur mainly from August to October [*Marenco et al.*, 1990; *Cooke et al.*, 1996; *Generoso et al.*, 2003; *Edwards et al.*, 2006b]. Figure 4 shows the BB areas from June to October 2007 as detected by MODIS. During the campaign period, the most important fire areas are located in the SH (South America, especially Brazil; southern Africa; and Madagascar). Note that only few fires occur in Southeast Asia during this period, although BB activity is noteworthy in Indonesia and Malaysia, especially in September. Figure 5 shows the variability of the 2007 CO partial columns corresponding to the three independent layers identified in section 2.1 (0–5 km, 5–11 km, and 11–17 km). The CO concentration increase, occurring from August as well as some peak increase occurring during September and October, is visible in the two lowest partial columns. Table 3 gives the CO concentration increase between the CO background value (calculated as the mean CO concentration from the beginning of the campaign to mid-July) and the mean CO concentration value at the end of the campaign (calculated as the mean CO concentration during the last 10 days of the campaign). Although CO is slightly more abundant in the 0–5 km layer at the beginning of the campaign, Table 3 shows that the 5–11 km layer is likely to present the most important CO increase (158.21% ± 65.77%). This CO increase seen in Figure 5 and mainly occurring above 5 km might be explained by the trade winds inversion occurring around 4 km above Reunion Island with easterly trade winds below 4 km and westerly flow above [*Taupin et al.*, 1999]. A more recent analysis based on GPS measurements over Reunion Island showed that the altitude of this inversion of wind direction depends on the season and varies between 3 km in austral winter and 5 km in austral summer [*Clain et al.*, 2009]. The westerly flow above the inversion enables transport of

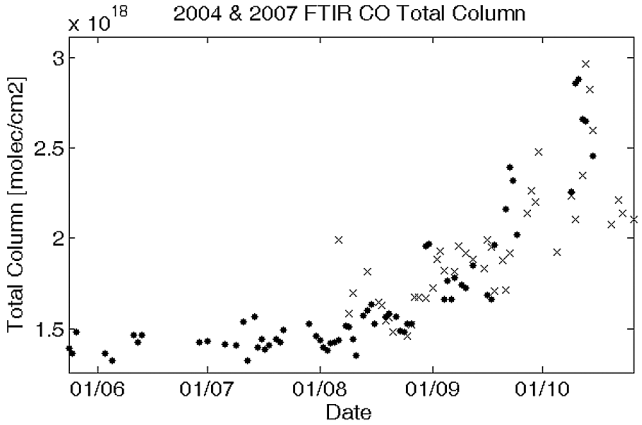

Figure 3. CO total columns (in molecules/cm^2) retrieved from the FTIR measurements during the 2004 (gray crosses) and 2007 (black dots) campaigns.

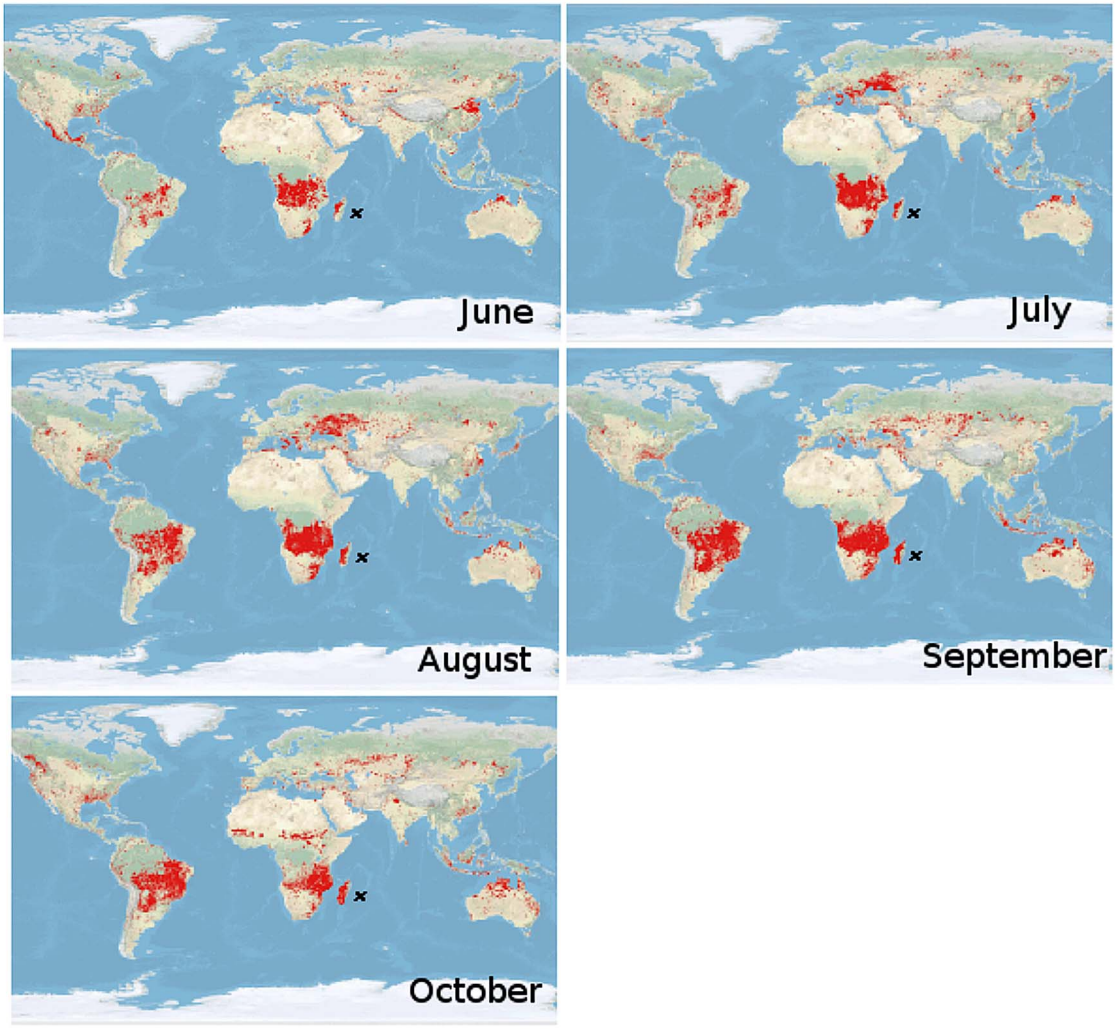

Figure 4. Active fires, shown in red, are detected using MODIS data on board the Terra satellite for June, July, August, September, and October 2007. Source: MODIS Rapid Response (http://rapidfire.sci.gsfc.nasa.gov/), Fire Information for Resource Management System (FIRMS) (http://maps.geog.umd.edu). Black crosses locate Reunion Island.

air masses coming from Africa and Madagascar which are enhanced in CO compared to easterly flow below the trade wind inversion.

[21] The CO partial column value in the 0–5 km layer at the beginning of the 2007 measurement campaign is relatively high ($5.51 \pm 0.56 \times 10^{17}$ molecules cm^{-2} which represents 67.78 ± 6.91 ppbv as a vmr value averaged over the whole partial column). The local air quality monitoring agency (Observatoire Réunionnais de l'Air (ORA), http://www.atmo-reunion.net/) indicates a mean ground CO vmr in Saint-Denis of around 110 ppbv. This CO concentration is measured close to the ground and is therefore more impacted by the local traffic pollution than the mean CO vmr given by the FTIR which is for the whole 0–5 km layer. The CO enhancement then visible in the 0–5 km layer (reaching by the end of the campaign $9.08 \pm 0.93 \times 10^{17}$ molecules cm^{-2} which represents 125.72 ± 12.82 ppbv as a vmr value averaged over the whole partial column) could come from dynamic exchanges between the low-tropospheric (0–5 km) and the midtropospheric (5–11 km) layers. This phenomenon has already been explained in the case of O_3 at Reunion Island [*Clain et al.*, 2009].

3.2. MOPITT Observations

[22] In order to analyze the variation in vertical CO distribution during the SH BB season, Figure 6 provides the monthly mean ratios between the 250 and 700 hPa MOPITT CO measurements from June to October 2007. A ratio value greater than 1 (smaller than 1) corresponds to more CO at the 250 hPa retrieval level than at the 700 hPa retrieval level (more CO at the 700 hPa retrieval level than at the 250 hPa retrieval level). No data are shown for cloudy pixels. For July, August, September, and October, the ratio value is small (~0.5) close to the continental source areas (southern Africa and South America). Ratio values around 0.7 can be observed in the known air transport pathway from South America and southern Africa to Australia (southern Atlantic Ocean and subtropical southern Indian Ocean) during the

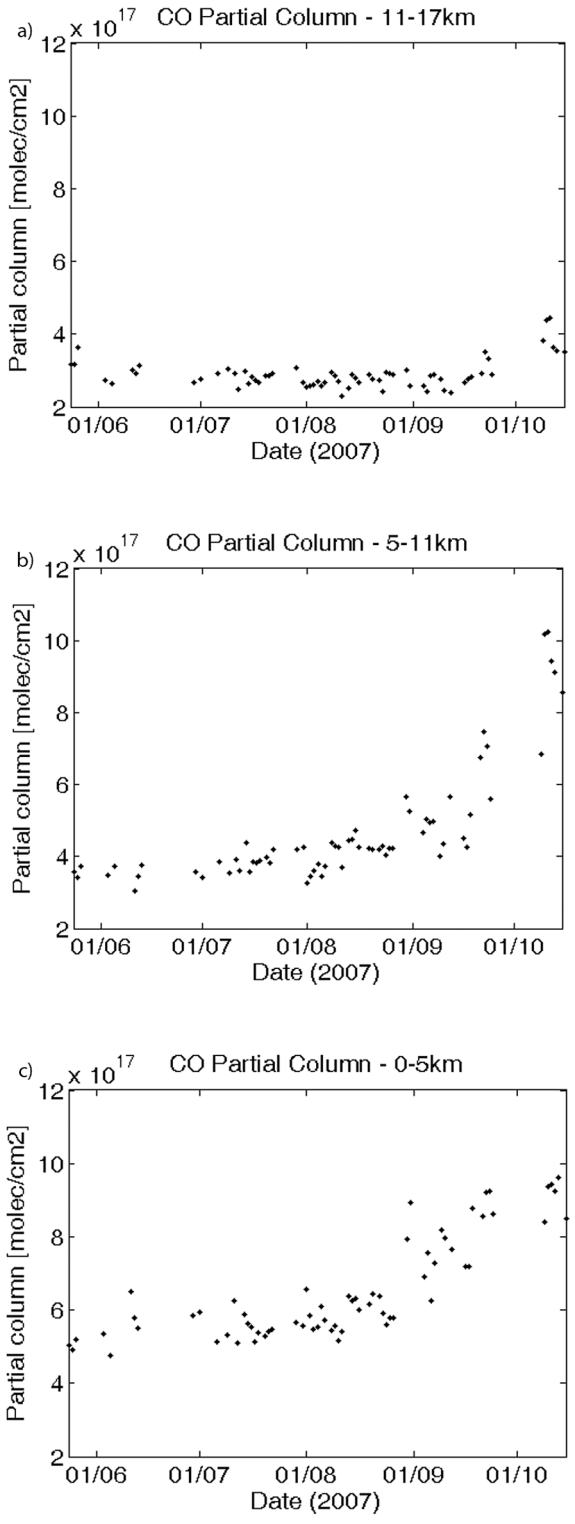

Figure 5. FTIR CO partial column's variability during the 2007 FTIR measurement campaign: (a) 11–17 km, (b) 5–11 km, and (c) 0–5 km.

whole period of study [*Edwards et al.*, 2006a]. While the BB activity increases, the ratio values in this long-range transport of CO over sea decrease from 0.8 in June and July to 0.6 in August, September, and October. The same observation can be made around Reunion Island, where the ratio values decrease from 0.9 to 0.7 during the period. Taking into consideration the MOPITT averaging kernels (Figure 2), it shows that CO-enriched air masses in this intercontinental transport pathway travel preferentially in the 700 hPa retrieval level, meaning in the ~2–8 km layer. Over the equatorial southern Indian Ocean, the 250/700 ratio values are much greater than 1 (~1.4) during the whole period of study and especially in June, July, and August, probably indicative for lifting boundary layer CO to high altitudes by deep convection over emission regions and subsequent transport. These results are discussed in the next section.

4. Origin of the Air Masses Passing Over Reunion Island

[23] The aim of this section is to identify the dynamical processes that govern the air masses transport to the Reunion Island areas and to identify the main potential source areas for CO-enriched air masses in the Reunion Island zone. The focus in this section is on the 2007 FTIR measurement campaign period (June to October). Figure 7 shows the areas defined and used for the following analysis: Area SAM stands for South America, area AFM stands for Africa and Madagascar, area SEA stands for Southeast Asia, area I-M stands for Indonesia and Malaysia, and area AUS stands for Australia. We calculated retroplumes using the Lagrangian particle dispersion model FLEXPART version 6.2 [*Stohl et al.*, 1998, 2005]. These calculations provide information on the origin of the air masses and give an estimate on the amount of time the air masses have spent in proximity to the Earth's surface. Knowledge of this residence time helps in identifying the potential contribution of each area to the CO concentration over Reunion Island. For our calculations we released 200,000 particles into each of the three layers identified in section 2.1 and corresponding to the FTIR partial columns (0–5 km, 5–11 km, and 11–17 km) over Reunion Island for each measurement day of the studied period (1 June to 31 October 2007). Each release lasted for 602 seconds, and each CO retroplume was traced back in time for 50 days. Figure 8 shows the geographical distribution of the mean residence time near the surface (<1000 m) in seconds of particles ending over Reunion Island in the 0–5 km, 5–11 km, and 11–7 km layers. Residence times are averaged per surface unit and per day. For the 0–5 km layer, the main potential contributive areas are areas SAM and AFM all along the period. The AFM contribution comes mainly from Madagascar and southern Africa. Also clearly visible is the roundabout pathway to the SAM region, where air masses leaving SAM gain altitude near Antarctica, descend again in the southern Indian Ocean where they ultimately arrive at Reunion from the southeast. For the 5–11 km layer, although potential contribution from areas SEA and I-M gain importance, areas SAM and AFM remain the main potential contributive areas for the whole period. This time AFM gains dominance over SAM and its main contributing areas shift to central Africa. There is no longer a clear indication of an arctic pathway to SAM, and indeed the LACYTRAJ simulations (see section 5) confirm that SAM contributions stem from more direct west to east pathways. For the 11–17 km layer, potential contributions of areas SEA and I-M clearly become prominent from June to September. Note also that

Table 3. CO Concentration Increase Between the CO Background Value and the Mean CO Concentration Value at the End of the Campaign for Each Partial Column During the 2007 Ground-Based FTIR Campaign[a]

Altitude Range (km)	CO Concentration (10^{17} molecules/cm^2)		CO Increase (%)
	Background	End of Campaign	
11–17	2.93 ± 0.53	3.89 ± 0.70	41.61 ± 49.17
5–11	3.63 ± 0.47	9.06 ± 1.17	158.21 ± 65.77
0–5	5.51 ± 0.56	9.08 ± 0.93	68.40 ± 34.00

[a]CO background value calculated as the mean CO concentration from the beginning of the campaign to mid-July. Mean CO concentration value at the end of the campaign calculated as the mean CO concentration during the ten last days of the campaign.

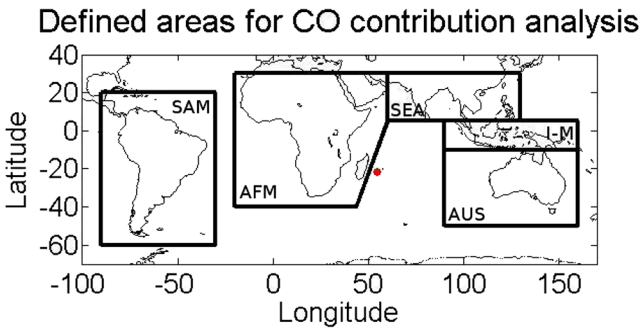

Figure 7. Areas defined and used for the CO contribution analysis. The measurement location (Reunion Island) is shown by the red dot.

the SEA and I-M air masses reaching the 11–17 km area have a strong residence time signature near the surface in the northern Indian Ocean, indicating that they get pushed upward by the southeastern lower-tropospheric (mostly SAM) and western (mostly AFM) flows into the upper troposphere. This process takes place relatively close to Reunion Island.

[24] Figure 9 shows the quantitative estimation of these residence times by area for each month and for each of the

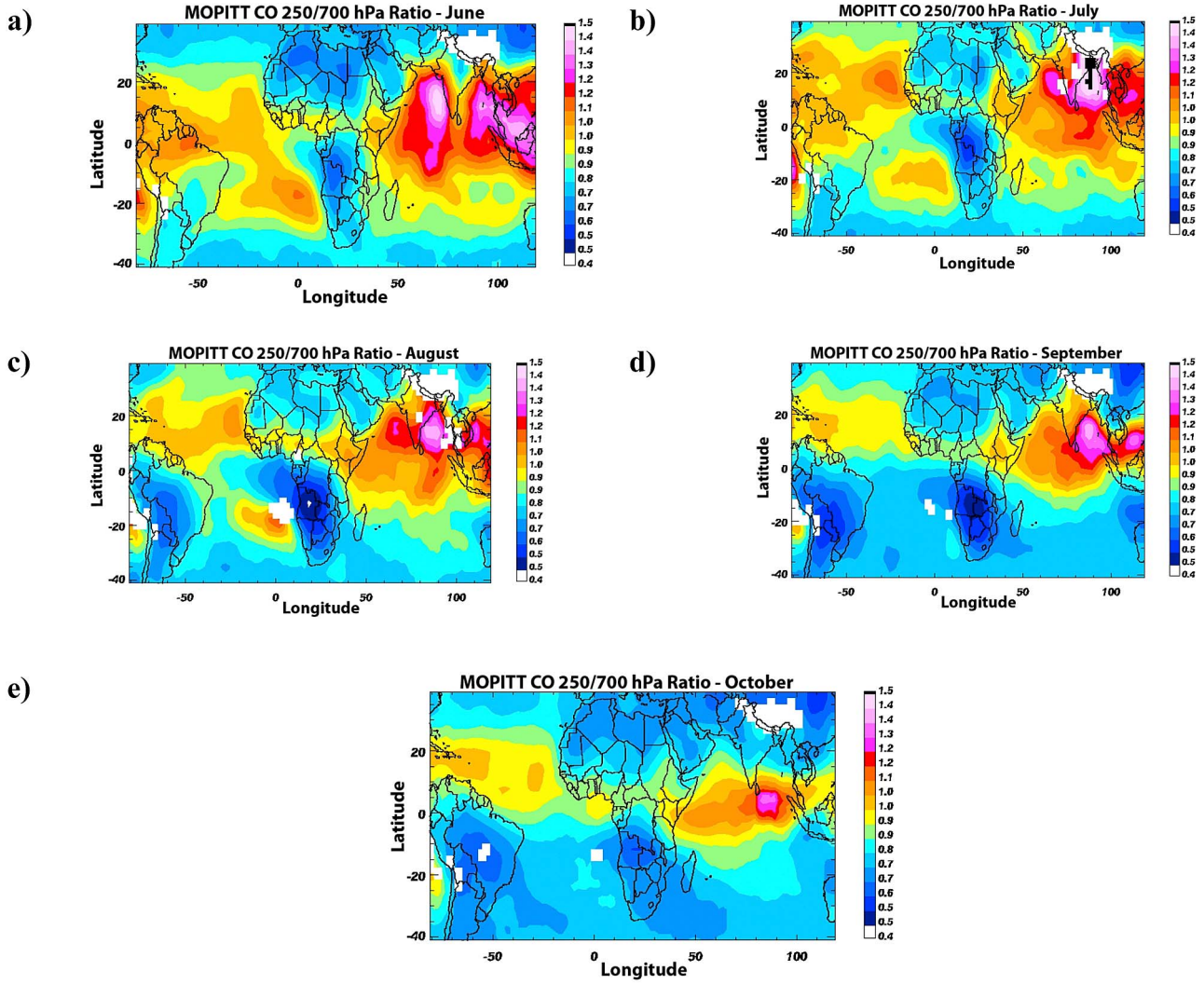

Figure 6. Monthly mean CO concentration ratios between 250 hPa and 700 hPa calculated from MOPITT CO retrievals for (a) June, (b) July, (c) August, (d) September, and (e) October 2007.

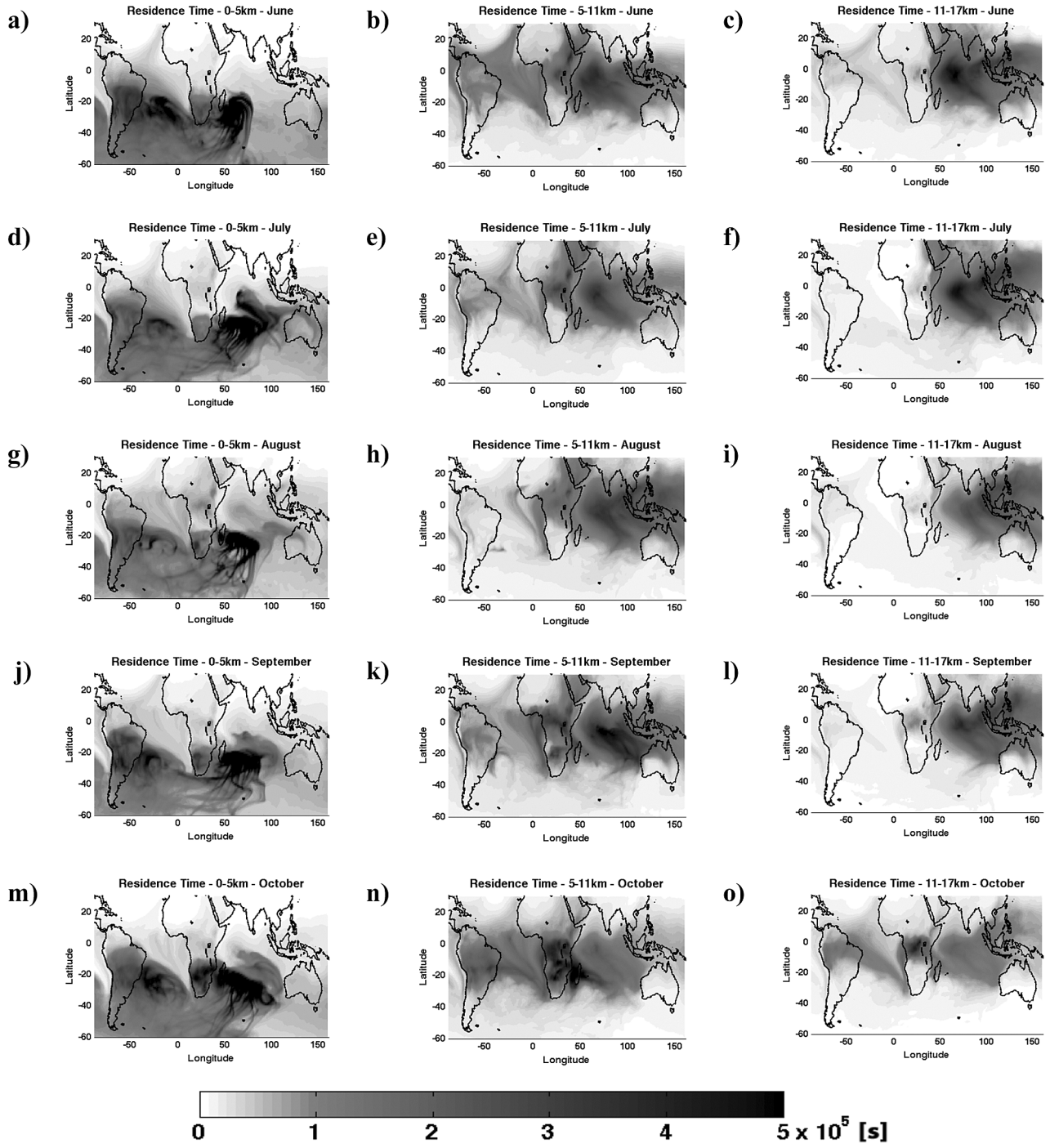

Figure 8. (left) Mean residence time of particles ending over Reunion Island in the 0–5 km layer during (a) June, (d) July, (g) August, (j) September, and (m) October 2007. (middle) Mean residence time of particles ending over Reunion Island in the 5–11 km layer during (b) June, (e) July, (h) August, (k) September, and (n) October 2007. (right) Mean residence time of particles ending over Reunion Island in the 11–17 km layer during (c) June, (f) July, (i) August, (l) September, and (o) October 2007. Color bar is limited to 5×10^5 s for clarity.

three partial columns. It confirms the main importance of areas SAM and AFM for the 0–5 km and 5–11 km layers for the whole period. However, areas SEA and I-M have mean residence times higher than the one of area SAM in August for the 5–11 km layer. For the 11–17 km layer and from June to September, potential contributions of areas SEA and I-M are more important than the potential contribution of area SAM and are even higher than the AFM potential con-

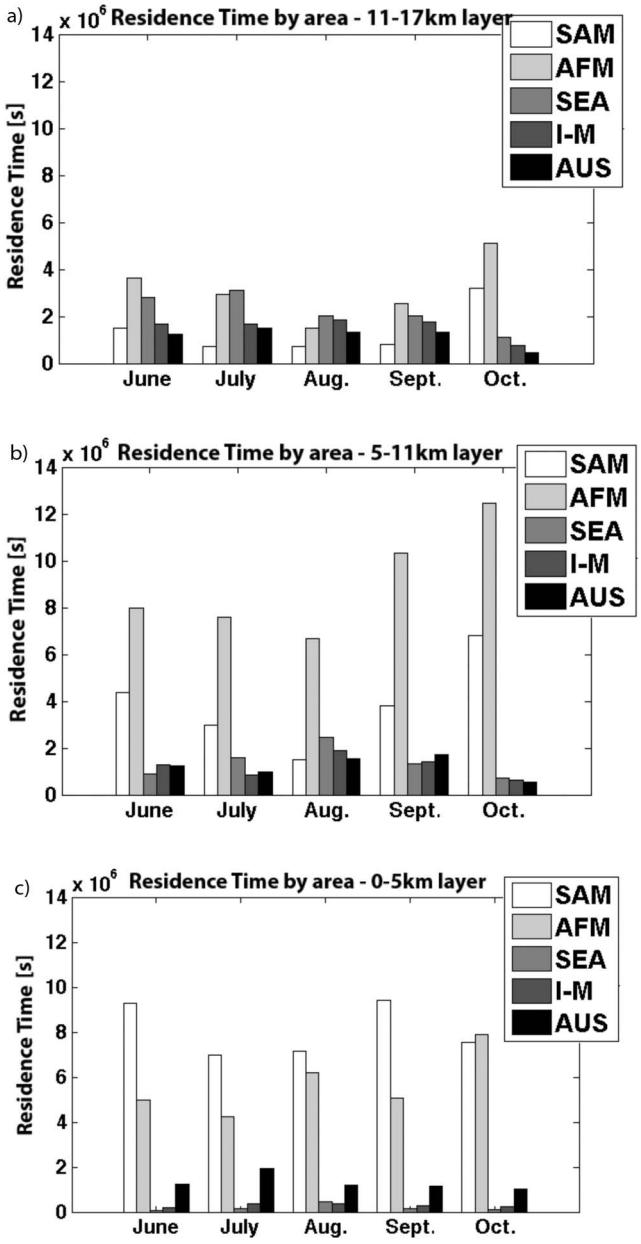

Figure 9. Mean residence time by area of particles ending over Reunion Island between June and October 2007. Back trajectories have been calculated over 50 days using FLEXPART for an ending in the (a) 11–17 km, (b) 5–11 km, and (c) 0–5 km layers.

tribution in August. Potential contribution of area SEA is also higher than the AFM potential contribution in July. Figure 10 shows the monthly evolution of the mean residence time over areas SEA + I-M of particles ending over Reunion Island in the 0–5 km, 5–11 km, and 11–17 km layers. The cumulative residence time of the three partial columns increases until its maximum in July and August and then decreases until its minimum in October. One can also notice that the residence times are the highest for particles ending in the 11–17 km layer, except in August when residence time for the 5–11 km layer is similar to the 11–17 km layer residence time. This might be related to the fact that the I-M SEA pathway remains close to the surface from a more prolonged period of time.

[25] To gain more insight into the processes taking place in the upper troposphere, we used LACYTRAJ to perform a set of back trajectories ending at Reunion Island at the 400 hPa (7 km), 300 hPa (9 km), and 200 hPa (12 km) levels (Figure 11). Each back trajectory has been computed over 10 days by LACYTRAJ during June, July, August, September, and October 2007. The 10 day duration for back trajectories is far enough to reach areas as far as South America. Each back trajectory has been superimposed to the other ones with a fixed transparency. The darkest regions are the ones over which pass the highest number of back trajectories. At the 300 and 400 hPa levels, the main crossed areas are clearly area AFM and area SAM, except in August for the 300 hPa level when a wide bundle of back trajectories comes from areas SEA and I-M. The westerly winds coming from Africa and South America are observable at the 400 and 300 hPa levels and agree well with the known air transport pathway from South America and southern Africa to Australia [*Edwards et al.*, 2006a]. At the 200 hPa level, one can notice that area SEA and area I-M are the second main air mass passing areas after area AFM, which confirms results from Figures 8 and 9. In October, Asian overpasses become less prominent while southern African and South American overpasses gain importance. It seems, therefore, that there is a "channel" linking Southeast Asia, Indonesia, and Malaysia to Reunion Island at 200 hPa from June to September which does not exist at the two lowest altitudes. This June to September channel would follow the main bundle of back trajectories shown on Figures 8c, 8f, and 8i. These observations are in accordance with the Asian monsoon anticyclone (AMA) seasonal cycle. During Northern Hemisphere summer, the AMA is the dominant circulation feature in the Indian-Asian upper troposphere lower-stratosphere (UTLS) region, located between 10°N and 40°N and forced by persistent deep convection coupled with circulation [*Hoskins and Rodwell*, 1995]. The strong anticyclonic circulation and the northeasterly winds blowing southeast of the AMA create favorable dynamic conditions to create the channel between

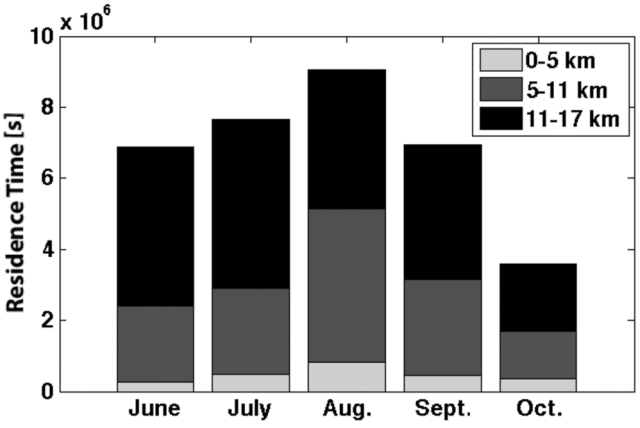

Figure 10. Evolution between June and October 2007 of the mean residence time over areas SEA + I-M of particles ending over Reunion Island in the 0–5 km, 5–11 km, and 11–17 km layers. Back trajectories have been calculated over 50 days using FLEXPART.

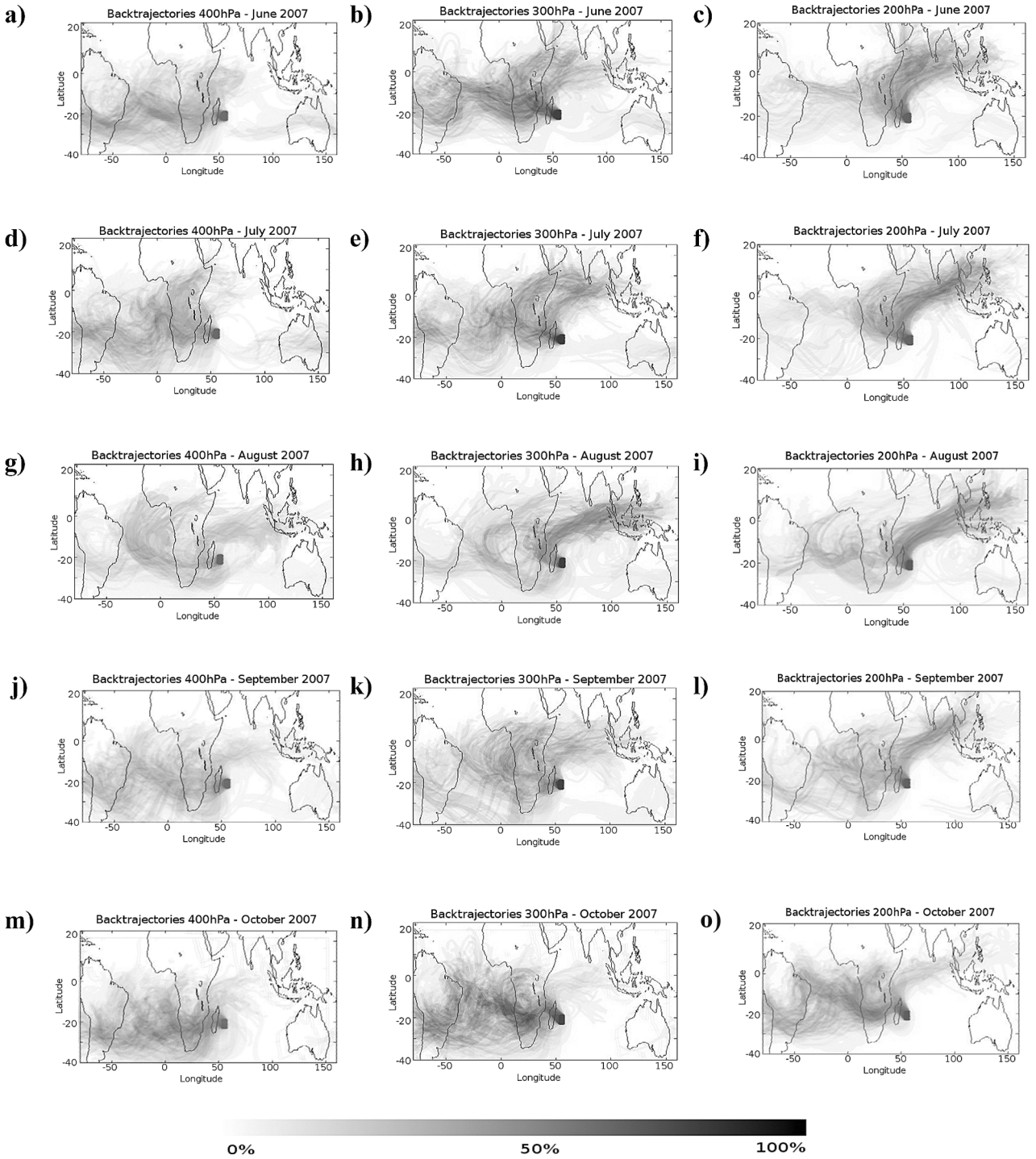

Figure 11. (left) LACYTRAJ 10 days back trajectories ending over Reunion Island at 400 hPa during (a) June, (d) July, (g) August, (j) September, and (m) October 2007. (middle) LACYTRAJ 10 days back trajectories ending over Reunion Island at 300 hPa during (b) June, (e) July, (h) August, (k) September, and (n) October 2007. (right) LACYTRAJ 10 days back trajectories ending over Reunion Island at 200 hPa during (c) June, (f) July, (i) August, (l) September, and (o) October 2007. Opacity gives occurrences.

Southeast Asia, Indonesia, Malaysia, and Reunion Island. Numerous recent studies have pointed out the strong uplift of boundary layer polluted air from India, Southeast Asia, and south China to the Asian UT during the ASM [*Li et al.*, 2001, 2005; *Lelieveld et al.*, 2002; *Fu et al.*, 2006; *Park et al.*, 2007; *Berthet et al.*, 2007]. In particular, within the monsoon anticyclone, UTLS CO can reach 140 ppbv at 200 hPa [*Li et al.*, 2005; *Park et al.*, 2007; *Barret et al.*, 2008]. This CO-enriched air mass could be then transported by the Hadley cell toward the subtropical southern Indian

Table 4. Vertical Distribution of the Emitted CO by Area According to the Fractional Distribution of Emission Heights for Wild Land Fires Recommended by *Dentener et al.* [2006]

Region	Tropical	Temperate	Eurasia	Canada
Latitude range	30°S; 30°N	60°S; 30°S 30°N; 60°N	60°N; 90°N	60°N; 90°N
Longitude range	180°W; 180°E	180°W; 180°E	30°E; 180°E	180°W; 30°E
Emitted CO in the 0–100 m range (%)	20	20	10	10
Emitted CO in the 100–500 m range (%)	40	20	10	10
Emitted CO in the 500–1000 m range (%)	40	20	20	10
Emitted CO in the 1000–2000 m range (%)	-	40	20	10
Emitted CO in the 2000–3000 m range (%)	-	-	40	20
Emitted CO in the 3000–6000 m range (%)	-	-	-	40

Ocean, in particular toward Reunion Island. This is in agreement with Figure 6 showing that CO concentrations at 250 hPa are greater than the 700 hPa CO concentrations between Southeast Asia and the subtropical southern Indian Ocean, especially from June to September.

5. Impact of CO-Enriched Air Masses on the CO Distribution Above Reunion Island

[26] In section 4, we pointed out the main potential source areas for CO-enriched air masses in the Reunion Island zone. We now want to investigate their impact on the locally observed CO concentrations. To do so, we used the calculated air mass folded residence time (in s m^3 kg^{-1}) with CO emissions (in kg m^{-3} s^{-1}) data from GFEDv2.1 for BB emissions and from EDGARv3.2-FT2000 for anthropogenic emissions (section 2.2.3). A mass mixing ratio (kg/kg) at the receptor point is then obtained and can be converted into partial column unit (molecules/cm^2). Table 4 shows how the emitted BB CO mass was distributed in altitude according to the fractional distribution of emission heights for wild land fires recommended in *Dentener et al.* [2006]. The anthropogenic emissions were distributed as follows: 20% between 0 and 100 m, 40% between 100 and 500 m, and 40% between 500 and 1000 m.

[27] Figure 12 shows the BB CO emitted by area from June to October for the year 2007 as well as the mean emitted BB CO from June to October over the years 2001 to 2006 according to GFEDv2.1 data. June to October anthropogenic CO emissions by area (EDGARv3.2-FT2000 data) are also given. While 2007 BB CO emissions by areas AFM, SEA, and AUS agree with their mean emissions over the 6 previous years, 2007 SAM BB emissions are especially high, and 2007 I-M BB emissions are especially low. The high SAM BB emissions can be explained by the fact that South America endured an especially high number of fires, in particular in Brazil, in the July–September period of 2007 [*Bevan et al.*, 2009; http://news.mongabay.com/2007/1021-amazon.html]. In total, CO emissions from areas SAM and AFM are the greatest ones, followed by emissions from areas SEA (mainly anthropogenic emissions), I-M, and AUS.

[28] Figure 13 shows the correlation between the total CO emitted and transported to Reunion Island as seen by FLEXPART (with GFEDv2.1 and EDGARv3.2-FT2000 data) versus the CO observed by FTIR in the partial column 0–17 km. The correlation coefficient is 0.94 (number of points is 64), showing that the CO enhancements simulated by the method described above are in line with the ground-based FTIR observations. Performing the same analysis on the three partial columns 0–5 km, 5–11 km, and 11–17 km, the correlation coefficients are 0.92, 0.87, and 0.82, respectively (not shown). The CO increase (calculated as the difference between the mean CO concentration during the

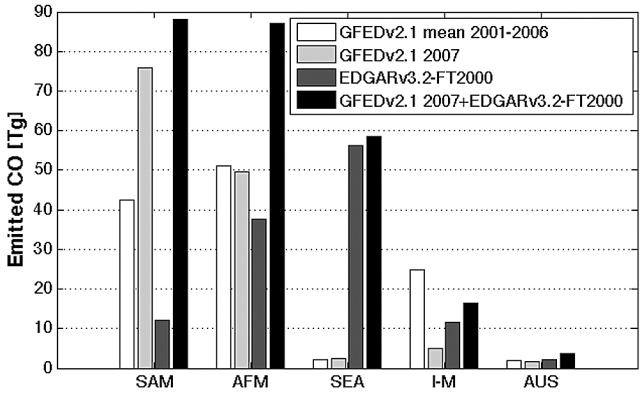

Figure 12. Mean emitted BB CO from June to October over the year 2001 to 2006 (GFEDv2.1 data), BB CO emitted by area from June to October 2007 (GFEDv2.1 data), and anthropogenic CO emitted from June to October 2000 (EDGARv3.2-FT2000 data). Emissions are given by area.

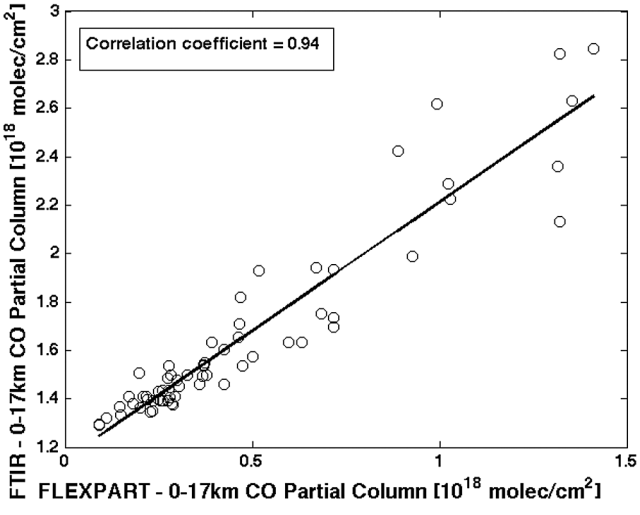

Figure 13. Correlation plot between the total BB (GFEDv2 data) and anthropogenic (EDGAR v3.2-FT2000) CO emitted and transported to Reunion Island as simulated by FLEXPART versus the CO observed by FTIR in the partial column 0–17 km for the June–October 2007 period. The correlation coefficient equals 0.94.

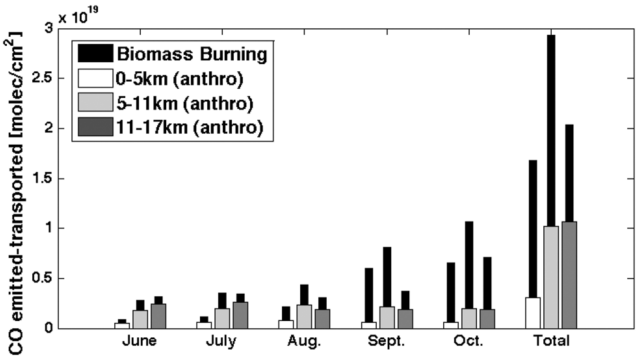

Figure 14. Cumulative BB (black bars) and anthropogenic (white and gray bars) CO concentration emitted/transported to Reunion Island in the 0–5 km, 5–11 km, and 11–17 km layers during the June to October 2007 period as inferred from FLEXPART simulations.

10 last days of the campaign and the mean CO concentration from the beginning of the campaign to mid-July) as simulated by FLEXPART equals 8.60×10^{17} molecules/cm^2, and the one observed by FTIR equals 9.96×10^{17} molecules/cm^2. This difference between the FLEXPART simulations and the ground-based FTIR observations can be due to the fact that the simulation does not include any chemical reactions. The oxidation source of CO from methane and other hydrocarbons is especially not considered.

[29] Figure 14 shows the cumulative BB and anthropogenic CO concentration emitted/transported to Reunion Island in the 0–5 km, 5–11 km, and 11–17 km layers during the June to October 2007 period as inferred from FLEXPART simulations. In total, the 5–11 km layer presents the most important CO increase, which agrees with the FTIR observations (section 3.1).

[30] Figure 15 shows the relative contribution of each of the areas defined in Figure 7 on the CO concentration at Reunion Island for each of the three partial columns. In the 0–5 km layer, area AFM is the main CO contributor for the whole period except in September and October when contribution from area SAM clearly increases because of the especially high 2007 wildfire activity in South America (Figure 12). The three remaining areas (SEA, I-M, and AUS) only have a small contribution in this low tropospheric layer. In the 5–11 km layer, area AFM is the main CO contributor during the whole period except in October when contribution from area SAM becomes larger. Areas SEA and I-M contribute more than in the 0–5 km layer, especially in August when their contributions are higher than the SAM area. These results confirm the predominance of the African and South American contributions in the CO concentration over Reunion Island below 11 km, because of the westerly winds (section 4) and the strength of BB (Figures 4 and 12).

[31] The situation is different in the 11–17 km layer: areas AFM and SAM are the two main contributors only in October. Moreover, from June to September, areas SEA and I-M are the two main contributors. In October, contributions from areas SAM and AFM increase while contributions from areas SEA and I-M decrease. Contribution in the CO concentration in Reunion Island from Southeast Asia and from Indonesia and Malaysia is then far more important in the 11–17 km layer than below 11 km, even outweighing the AFM contribution from June to September, whereas SEA and I-M CO emissions are below the AFM ones (Figure 12). This confirms the dynamic analysis (section 4) showing a pathway between Southeast Asia, Indonesia, and Malaysia and the subtropical southern Indian Ocean in the upper troposphere from June to September. Furthermore, this upper tropospheric long-range transport of CO is in agreement with the values of the monthly mean ratios of MOPITT CO retrievals between 250 hPa and 700 hPa which are greater than 1 along this pathway in June, July, and August (Figure 6). However, the 250/700 ratio over Reunion Island remains lower than 1 (~0.9) during this period, showing a greater CO concentration in the lower troposphere than in the upper troposphere. This is due to the mixing with CO-enriched air masses coming from Africa/Madagascar and South America travelling in the lower troposphere.

[32] While Southeast Asia and Indonesia-Malaysia are significantly contributing areas, Australia remains the zone which contributes the least for the whole SH BB season and for the whole troposphere.

[33] One can also notice in Figure 15 the importance of the transport of CO from South America, especially in October when this source dominates the African source in the three partial columns. This is explained by the especially high 2007 South American BB CO emissions (Figure 11).

[34] We thus infer that the Australian emission sources contribute little to the CO concentration observed over Reunion Island. The main contributors to the CO variations are southern Africa and South America throughout the entire column, and also Southeast Asia, Indonesia, and Malaysia in the 11–17 km layer from June to September. Given the low I-M BB CO emissions during the 2007 SH BB season compared to the mean emissions over the 6 previous years (Figure 12), this I-M upper tropospheric contribution could be more important during other years.

6. Conclusions

[35] The objectives of this paper were to document the evolution of the vertical distribution of the abundance of CO above Reunion Island with time and to determine the sources which govern this evolution. We have focused especially on the impact of CO-enhanced air masses coming from Southeast Asia, Indonesia, and Malaysia on the CO distribution in the subtropical southern Indian Ocean area.

[36] Data from an FTIR campaign performed in 2007 indicate a doubling of CO total columns in the course of the SH BB season, consistent with measurements from a similar campaign that took place in 2004. The influence of different source areas (southern Africa, South America, Southeast Asia, Indonesia and Malaysia, and Australia) has been discussed using LACYTRAJ back trajectory analyses and FLEXPART modeling combined with GFEDv2.1 fire emission data and EDGARv3.2-FT2000 anthropogenic emission data for CO. The main sources of CO for Reunion Island in austral spring are southern Africa and South America. We have shown that the areas of Southeast Asia and Indonesia-Malaysia are potential extra sources for CO in the upper troposphere, especially in July and August, when upper tropospheric dynamical conditions are propitious to bring into being a channel linking Southeast Asia to the southern Indian

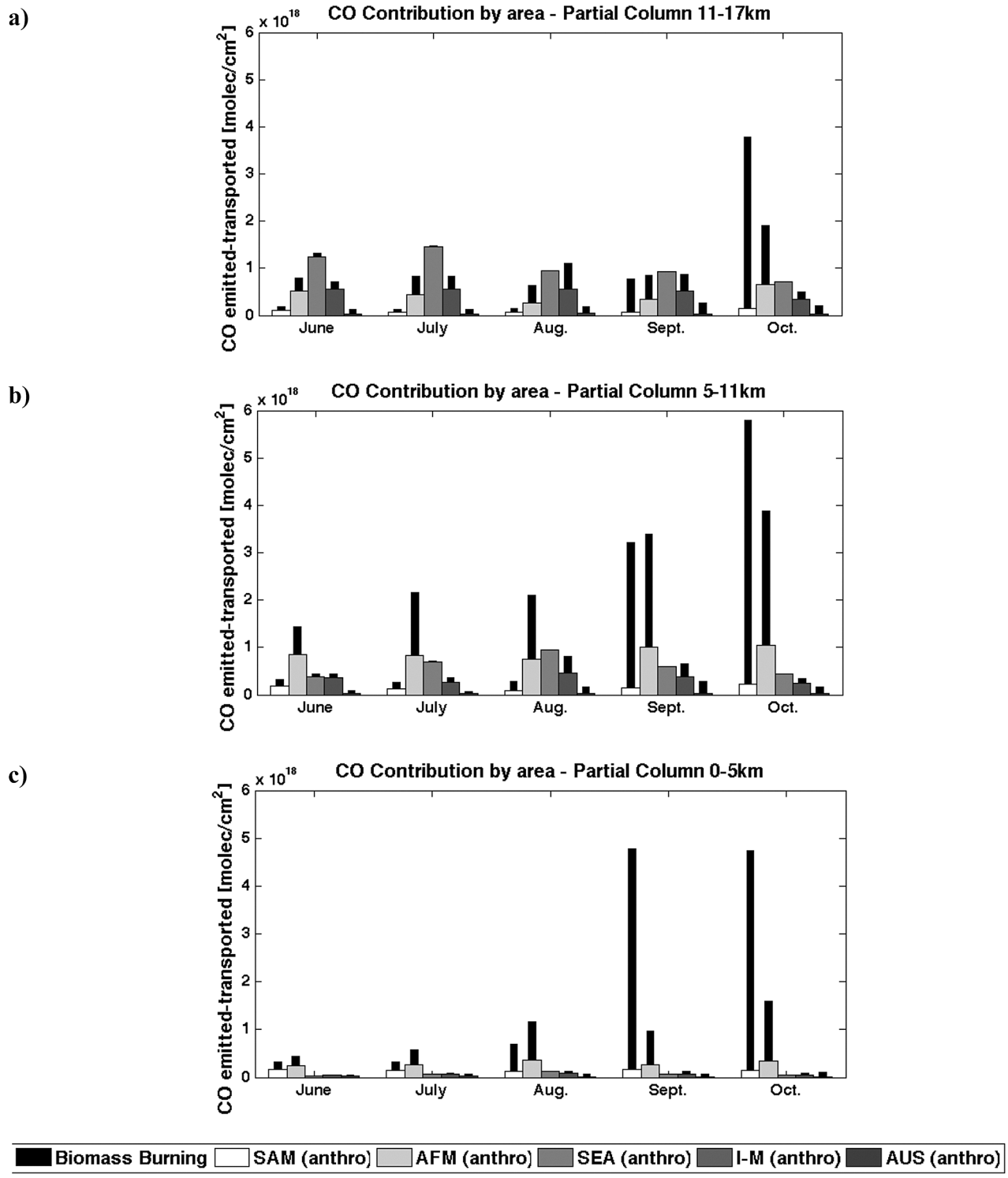

Figure 15. Cumulative BB (black bars) and anthropogenic (white and gray bars) CO concentration emitted/transported to Reunion Island by area in the (a) 11–17 km layer, (b) 5–11 km layer, and (c) 0–5 km layer for June, July, August, September, and October 2007 as inferred from FLEXPART simulations.

Ocean. We have shown that in the upper tropospheric layer (11–17 km) from June to September, Southeast Asia and Indonesia-Malaysia are the main contributing areas to the CO enhancement occurring in the subtropical southern Indian Ocean. This is, therefore, a new identified long-range transport pathway of CO significantly affecting the subtropical southern Indian Ocean area.

[37] Our further objective is now to establish continuous FTIR measurements in order to complete the characterization of the CO distribution over Reunion Island over a longer measurement period thanks to the permanent installation of the ground-based FTIR since May 2009 in Reunion Island. We also plan to extend the study to other pollutants emitted from BB, including observation of aerosols by lidar over Reunion Island and in the Indian Ocean with additional shipborne lidar campaign measurements in the Mozambique Channel, toward the Kerguelen Islands and close to Indonesia.

[38] **Acknowledgments.** The authors thank the French regional, national (INSU, CNRS), and international (NASA/GFSC) organizations for supporting the OPAR (Observatoire de Physique de l'Atmosphère de la Réunion) station. The Centre National de Recherche Scientifique (CNRS) and the Agence de l'Environnement et de la Maîtrise de l'Energie (ADEME) provide funding to V. Duflot for his Ph.D. The FTIR campaigns at Reunion and FLEXPART analyses are supported by the Belgian Science Policy via the Science for a Sustainable Development program (contract AGACC) and the ESA/PRODEX program (contract SECPEA), as well as by the EU project SCOUT-O3. MOPITT mission and data analysis are supported by the Canadian Space Agency, the Natural Sciences and Engineering Research Council (NSERC), and the National Aeronautics and Space Administration (NASA). MOPITT retrievals are performed by NCAR. We thank the ECMWF center for supplying global model data. We thank the MODIS team (NASA) and the University of Maryland for providing fires detection data. We also wish to thank the Observatoire Réunionnais de l'Air (ORA) for local ground CO concentration data. Jean-Marc Metzger (OPAR), Francis Scolas, and Christian Hermans (BIRA-IASB) also receive our gratitude for supporting the FTIR operation.

References

Annegarn, H. J., L. Otter, R. J. Swap, and R. J. Scholes (2002), Southern Africa's ecosystem in a test-tube: A perspective on the Southern African Regional Science Initiative (SAFARI 2000), *S. Afr. J. Sci.*, *98*, 111–113.

Baray, J. L., G. Ancellet, F. G. Taupin, M. Bessafi, S. Baldy, and P. Keckhut (1998), Subtropical tropopause break as a possible stratospheric source of O_3 in the tropical troposphere, *J. Atmos. Sol. Terr. Phys.*, *60*(1), 27–36.

Barret, B., et al. (2008), Transport pathways of CO in the African upper troposphere during the monsoon season: A study based upon the assimilation of spaceborne observations, *Atmos. Chem. Phys.*, *8*, 3231–3246.

Berthet, G., J. G. Esler, and P. H. Haynes (2007), A Lagrangian perspective of the tropopause and the ventilation of the lowermost stratosphere, *J. Geophys. Res.*, *112*, D18102, doi:10.1029/2006JD008295.

Bevan, S. L., P. R. J. North, W. M. F. Grey, S. O. Los, and S. E. Plummer (2009), Impact of atmospheric aerosol from biomass burning on Amazon dry-season drought, *J. Geophys. Res.*, *114*, D09204, doi:10.1029/2008JD011112.

Bremer, H., et al. (2004), Spatial and temporal variation of MOPITT CO in Africa and South America: A comparison with SHADOZ ozone and MODIS aerosol, *J. Geophys. Res.*, *109*, D12304, doi:10.1029/2003JD004234.

Clain, G., J. L. Baray, R. Delmas, R. Diab, J. Leclair de Bellevue, P. Keckhut, F. Posny, J. M. Metzger, and J. P. Cammas (2009), Tropospheric O_3 climatology at two Southern Hemisphere tropical/subtropical sites, (Reunion Island and Irene, South Africa) from ozonesondes, LIDAR, and in situ aircraft measurements, *Atmos. Chem. Phys.*, *9*, 1723–1734.

Clain, G., J. L. Baray, R. Delmas, P. Keckhut, and J.-P. Cammas (2010), A Lagrangian approach to analyse the tropospheric ozone climatology in the tropics: Climatology of stratosphere-troposphere exchange at Reunion Island, *Atmos. Environ.*, *44*, 968–975.

Cooke, W. F., B. Koffi, and J. M. Grégoire (1996), Seasonality of vegetation fires in Africa from remote sensing data and application to a global chemistry model, *J. Geophys. Res.*, *101*, 21,051–21,065.

Daniel, J. S., and S. Solomon (1998), On the climate forcing of carbon monoxide, *J. Geophys. Res.*, *103*, 13,249–13,260.

Deeter, M. N., L. K. Emmons, D. P. Edwards, J. C. Gille, and J. R. Drummond (2004a), Vertical resolution and information content of CO profiles retrieved by MOPITT, *Geophys. Res. Lett.*, *31*, L15112, doi:10.1029/2004GL020235.

Deeter, M. N., et al. (2004b), Evaluation of operational radiances for the Measurements of Pollution in the Troposphere (MOPITT) instrument CO thermal band channels, *J. Geophys. Res.*, *109*, D03308, doi:10.1029/2003JD003970.

Deeter, M. N., D. P. Edwards, J. C. Gille, and J. R. Drummond (2007), Sensitivity of MOPITT observations to carbon monoxide in the lower troposphere, *J. Geophys. Res.*, *112*, D24306, doi:10.1029/2007JD008929.

De Laat, A. T. J., J. Lelieveld, G. J. Roelofs, R. R. Dickerson, and J. M. Lobert (2001), Source analysis of carbon monoxide pollution during INDOEX 1999, *J. Geophys. Res.*, *106*, 28,481–28,495.

Dentener, F., et al. (2006), Emissions of primary aerosol and precursor gases in the years 2000 and 1750 prescribed data-sets for AeroCom, *Atmos. Chem. Phys.*, *6*, 4321–4344.

Drummond, J. R., and G. S. Mand (1996), The Measurements of Pollution in the Troposphere (MOPITT) instrument, Overall performance and calibration requirements, *J. Atmos. Oceanic Technol.*, *13*, 314–320.

Edwards, D. P., et al. (2006a), Satellite-observed pollution from Southern Hemisphere biomass burning, *J. Geophys. Res.*, *111*, D14312, doi:10.1029/2005JD006655.

Edwards, D. P., G. Pétron, P. C. Novelli, L. K. Emmons, J. C. Gille, and J. R. Drummond (2006b), Southern Hemisphere carbon monoxide interannual variability observed by Terra/Measurement of Pollution in the Troposphere (MOPITT), *J. Geophys. Res.*, *111*, D16303, doi:10.1029/2006JD007079.

Emmons, L. K., et al. (2004), Validation of Measurements of Pollution in the Troposphere (MOPITT) CO retrievals with aircraft in situ profiles, *J. Geophys. Res.*, *109*, D03309, doi:10.1029/2003JD004101.

Emmons, L. K., G. G. Pfister, D. P. Edwards, J. C. Gille, G. Sachse, D. Blake, S. Wofsy, C. Gerbig, D. Matross, and P. Nédélec (2007), Measurements of Pollution in the Troposphere (MOPITT) validation exercises during summer 2004 field campaigns over North America, *J. Geophys. Res.*, *112*, D12S02, doi:10.1029/2006JD007833.

Emmons, L. K., D. P. Edwards, M. N. Deeter, J. C. Gille, T. Campos, P. Nédélec, P. Novelli, and G. Sachse (2009), Measurements of Pollution In The Troposphere (MOPITT) validation through 2006, *Atmos. Chem. Phys.*, *9*, 1795–1803.

Fu, R., Y. Hu, J. S. Wright, J. H. Jiang, R. E. Dickinson, M. Chen, M. Filipiak, W. G. Read, J. W. Waters, and D. L. Wu (2006), Short circuit of water vapor and polluted air to the global stratosphere by convective transport over the Tibetan Plateau, *Proc. Natl. Acad. Sci. U. S. A.*, *103*, 5664–5669.

Galanter, M., H. Levy, and G. R. Carmichael (2000), Impacts of biomass burning on tropospheric CO, NO_x, and O_3, *J. Geophys. Res.*, *105*, 6633–6653.

Garstang, M., P. D. Tyson, R. Swap, M. Edwards, P. Kallberg, and J. A. Lindesay (1996), Horizontal and vertical transport of air over southern Africa, *J. Geophys. Res.*, *101*, 23,721–23,736.

Generoso, S., F.-M. Bréon, Y. Balkanski, O. Boucher, and M. Schulz (2003), Improving the seasonal cycle and interannual variations of biomass burning aerosol sources, *Atmos. Chem. Phys.*, *3*, 1211–1222.

Giglio, L., J. Descloitres, C. O. Justice, and Y. J. Kaufman (2003), An enhanced contextual fire detection algorithm for MODIS, *Remote Sens. Environ.*, *87*, 273–282.

Hoskins, B. J., and M. J. Rodwell (1995), A model of the Asian summer monsoon. Part I: the global scale, *J. Atmos. Sci.*, *52*, 1329–1340.

Intergovernmental Panel on Climate Change (2001), *Climate Change 2001*, edited by J. T. Houghton et al., Cambridge Univ. Press, New York.

Kanakidou, M., and P. J. Crutzen (1999), The photochemical source of carbon monoxide: Importance, uncertainties and feedbacks, *Chemosphere*, *1*, 91–109.

Kar, J., et al. (2004), Evidence of vertical transport of carbon monoxide from Measurements of Pollution in the Troposphere (MOPITT), *Geophys. Res. Lett.*, *31*, L23105, doi:10.1029/2004GL021128.

Leclair De Bellevue, J., A. Réchou, J. L. Baray, G. Ancellet, and R. D. Diab (2006), Signatures of stratosphere to troposphere transport near deep convective events in the southern subtropics, *J. Geophys. Res.*, *111*, D24107, doi:10.1029/2005JD006947.

Lelieveld, J., et al. (2002), Global air pollution crossroads over the Mediterranean, *Science*, *298*, 794–799.

Li, Q. L., et al. (2001), A tropospheric ozone maximum over the Middle East, *Geophys. Res. Lett.*, *28*(D17), 3235–3238.

Li, Q. L., et al. (2005), Convective outflow of South Asian pollution: A global CTM simulation compared with EOS MLS observations, *Geophys. Res. Lett.*, *32*, L14826, doi:10.1029/2005GL022762.

Logan, J. A., M. J. Prather, S. C. Wofsy, and M. B. McElroy (1981), Tropospheric chemistry: A global perspective, *J. Geophys. Res.*, *86*, 7210–7254.

Marenco, A., J. C. Medale, and S. Prieur (1990), Study of tropospheric ozone in the tropical belt (Africa, America) from STRATOZ and TROPOZ campaigns, *Atmos. Environ.*, *11*, 2823–2834.

McMillan, W. W., et al. (2003), Tropospheric carbon monoxide measurements from the Scanning High-Resolution Interferometer Sounder on 7 September 2000 in southern Africa during SAFARI 2000, *J. Geophys. Res.*, *108*(D13), 8492, doi:10.1029/2002JD002335.

Olivier, J., J. Van Aardenne, F. Dentener, V. Pagliari, L. Ganzeveld, and J. Peters (2005), Recent trends in global greenhouse gas emissions: Regional trends 1970–2000 and spatial distribution of key sources in 2000, *Environ. Sci.*, *2*(2), 81–99.

Pak, B. C., et al. (2003), Measurements of biomass burning influences in the troposphere over southeast Australia during the SAFARI 2000 dry season campaign, *J. Geophys. Res.*, *108*(D13), 8480, doi:10.1029/2002JD002343.

Park, M., W. J. Randel, A. Gettelman, S. T. Massie, and J. H. Jiang (2007), Transport above the Asian summer monsoon anticyclone inferred from Aura Microwave Limb Sounder tracers, *J. Geophys. Res.*, *112*, D16309, doi:10.1029/2006JD008294.

Randriambelo, T., J. L. Baray, and S. Baldy (2000), The effect of biomass burning, convective venting, and transport on tropospheric O_3 over the Indian ocean: Reunion Island field observations, *J. Geophys. Res.*, *105*(D9), 11,813–11,832.

Ridley, B. A., S. Madronich, R. B. Chatfield, J. G. Walega, R. E. Shetter, M. A. Carroll, and D. D. Montzka (1992), Measurements and model simulations of the photostationary state during the Mauna Loa Observatory Photochemistry Experiment: Ozone production and loss rates, *J. Geophys. Res.*, *97*, 10,275–10,388.

Rodgers, C. (2000), *Inverse Methods for Atmospheric Sounding: Theory and Practice*, *Series on Atmospheric, Oceanic and Planetary Physics*, vol. 2, World Sci., Singapore.

Senten, C., et al. (2008), Technical Note: New ground-based FTIR measurements at Ile de La Réunion: Observations, error analysis, and comparisons with independent data, *Atmos. Chem. Phys.*, *8*, 3483–3508.

Stohl, A., and D. J. Thomson (1999), A density correction for Lagrangian particle dispersion models, *Boundary Layer Meteorol.*, *90*(1), 155–167.

Stohl, A., M. Hittenberger, and G. Wotawa (1998), Validation of the Lagrangian particle dispersion model FLEXPART against large-scale tracer experiment data, *Atmos. Environ.*, *32*, 4245–4264.

Stohl, A., C. Forster, A. Frank, P. Seibert, and G. Wotawa (2005), Technical note: The Lagrangian particle dispersion model FLEXPART version 6.2., *Atmos. Chem. Phys.*, *5*, 2461–2474.

Swap, R. J., H. J. Annegarn, J. T. Suttles, M. D. King, S. Platnick, J. L. Privette, and R. J. Scholes (2003), Africa burning: A thematic analysis of the South African Regional Science Initiative (SAFARI 2000), *J. Geophys. Res.*, *108*(D13), 8465, doi:10.1029/2003JD003747.

Taupin, F. G., M. Bessafi, S. Baldy, and P. J. Bremaud (1999), Tropospheric O_3 above the southwestern Indian Ocean is strongly linked to dynamical conditions prevailing in the tropics, *J. Geophys. Res.*, *104* (D7), 8057–8066.

Thompson, A. M. (1992), The oxidizing capacity of the Earth's atmosphere: Probable past and future changes, *Science*, *256*, 1157–1165.

van der Werf, G. R., J. T. Randerson, L. Giglio, G. J. Collatz, P. S. Kasibhatla, and A. F. Arellano Jr. (2006), Interannual variability in global biomass burning emission from 1997 to 2004, *Atmos. Chem. Phys.*, *6*, 3423–3441.

Vigouroux, C., et al. (2009), Ground-based FTIR and MAX-DOAS observations of formaldehyde at Réunion Island and comparisons with satellite and model data, *Atm. Chem. Phys. Disc.*, *9*, 15,891–15,957.

Zachariasse, M., P. van Velthoven, H. Smit, J. Lelieveld, T. Mandal, and H. Kelder (2000), Influence of stratosphere-troposphere exchange on tropospheric ozone over the tropical Indian Ocean during the winter monsoon, *J. Geophys. Res.*, *105*(D12), 15,403–15,416.

J. L. Attié, Laboratoire d'Aérologie, UMR 5560, Université de Toulouse, CNRS/UPS, F-31400 Toulouse, France.

J. L. Baray, G. Clain, R. Delmas, and V. Duflot, Laboratoire de l'Atmosphère et des Cyclones, Université de la Réunion, UMR CNRS-Météo-France 8105, F-97715 Saint-Denis de la Réunion, France. (vduflot@univ-reunion.fr)

M. De Mazière, B. Dils, C. Senten, G. Vanhaelewyn, and C. Vigouroux, Institut d'Aéronomie Spatiale de Belgique, 3 Av. Circulaire, B-1180 Bruxelles, Belgium.